Structural and Molecular Characterization of a Preferred Protein Interaction Surface on G Protein $\beta\gamma$ Subunits†

Tara L. Davis,‡,§ Tabetha M. Bonacci,‡,|| Stephen R. Sprang,*,§,⊥ and Alan V. Smrcka*,||,#

Department of Biochemistry and The Howard Hughes Medical Institute, University of Texas Southwestern Medical Center, 5323 Harry Hines Boulevard, MC 9050, Dallas, Texas 75390-9050, and Department of Pharmacology and Physiology and Department of Biochemistry and Biophysics, University of Rochester School of Medicine and Dentistry, Box 711, 601 Elmwood Avenue, Rochester, New York 14642

Received April 9, 2005; Revised Manuscript Received June 13, 2005

ABSTRACT: G protein $\beta\gamma$ subunits associate with many binding partners in cellular signaling cascades. In previous work, we used random-peptide phage display screening to identify a diverse family of peptides that bound to a common surface on G$\beta\gamma$ subunits and blocked a subset of G$\beta\gamma$ effectors. Later studies showed that one of the peptides caused G protein activation through a novel G$\beta\gamma$-dependent, nucleotide exchange-independent mechanism. Here we report the X-ray crystal structure of G$\beta_1\gamma_2$ bound to this peptide, SIGK (SIGKAFKILGYPDYD), at 2.7 Å resolution. SIGK forms a helical structure that binds the same face of Gβ_1 as the switch II region of Gα. The interaction interface can be subdivided into polar and nonpolar interfaces that together contain a mixture of binding determinants that may be responsible for the ability of this surface to recognize multiple protein partners. Systematic mutagenic analysis of the peptide−Gβ_1 interface indicates that distinct sets of amino acids within this interface are required for binding of different peptides. Among these unique amino acid interactions, specific electrostatic binding contacts within the polar interface are required for peptide-mediated subunit dissociation. The data provide a mechanistic basis for multiple target recognition by G$\beta\gamma$ subunits with diverse functional interactions within a common interface and suggest that pharmacological targeting of distinct regions within this interface could allow for selective manipulation of G$\beta\gamma$-dependent signaling pathways.

Heterotrimeric G proteins are composed of α, β, and γ subunits; the β and γ subunits tightly associate and exist as a constitutive dimer. Gα, when bound to GDP, has a high affinity for G$\beta\gamma$, forming a heterotrimer in which neither component can signal to its downstream targets. In the classical model for activation of G protein signaling cascades, ligand binding activates G protein coupled receptors that catalyze exchange of GDP for GTP on the Gα subunit. Gα bound to GTP dissociates from G$\beta\gamma$, freeing both subunits to interact with effector molecules (*1*, *2*). Recently, a new class of regulators, AGS[1] proteins (activator of G protein signaling), has been identified which activate G protein signaling in the absence of nucleotide exchange (*3*).

G$\beta\gamma$ subunits signal to an array of effector molecules, including enzymes and ion channels, and mediate various physiological and cellular functions (*4*). Since Gα subunits block G$\beta\gamma$ regulation of most effector targets, it was hypothesized that effector interaction sites overlap with the Gα subunit interaction interface. Indeed, mutation of amino acids important for Gα binding altered effector regulation (*5*, *6*), but mutations to other areas outside the Gα−G$\beta\gamma$ interface also impaired effector regulation (*7*−*9*).

To probe the nature of protein interaction surfaces on G$\beta\gamma$, we screened random-peptide phage display libraries against G$\beta_1\gamma_2$ subunits to identify G$\beta\gamma$ binding sequences (*10*). The screen yielded a series of peptide sequences that, despite their sequence diversity, apparently bound to a single surface on G$\beta\gamma$. We hypothesized that this surface was a protein−protein interaction "hot spot", defined as an area on a protein surface that has properties especially favorable for mediating

† This work was supported by NIH Grants GM60286 (A.V.S.) and DK46371 (S.R.S.), Welch Foundation Grant I-1229 (S.R.S.), The John W. and Rhonda K. Pate Professorship (S.R.S.), NIH Predoctoral Training Grant in Cardiovascular Biology HLT3207949 (T.M.B.), and NIH Predoctoral Training Grant T32GM8297 (T.L.D.).

* To whom correspondence should be addressed. S.R.S.: tel, 214-645-5930; fax, 214-648-6336; e-mail, Stephen.Sprang@utsouthwestern.edu. A.V.S.: tel, 585-275-0892; fax, 585-273-2652; e-mail, Alan_Smrcka@urmc.rochester.edu.

‡ These authors contributed equally to this work.

§ Department of Biochemistry, University of Texas Southwestern Medical Center.

|| Department of Pharmacology and Physiology, University of Rochester School of Medicine and Dentistry.

⊥ The Howard Hughes Medical Institute, University of Texas Southwestern Medical Center.

Department of Biochemistry and Biophysics, University of Rochester School of Medicine and Dentistry.

[1] Abbreviations: GDP, guanosine diphosphate; GTP, guanosine triphosphate; $C_{12}E_{10}$, polyoxyethylene 10 lauryl ether; AGS, activator of G protein signaling; GRK, G protein coupled receptor kinase; PI3K, phosphatidylinositol 3-kinase; ERK, extracellular signal-regulated protein kinase; QEHA, QEHAQEPERQYMHIGTMVEFAYALVGK; βark-ct peptide, WKKELRTMGEEDFFDLLASKSQSKRMDDQRVDLAG; PLC, phospholipase C; AC, adenylyl cyclase; bG$\beta_1\gamma_2$, biotinylated G$\beta_1\gamma_2$; TBS, Tris-buffered saline; HRP, horseradish peroxidase; ABTS, 2,2′-azinobis(3-ethylbenzothiazoline)-6-sulfonic acid; EDTA, ethylenediaminetetraacetic acid; HEPES, 4-(2-hydroxyethyl)-1-piperazineethanesulfonic acid; CNS, crystallography and NMR system; CHAPS, 3-[(3-cholamidopropyl)dimethylammonio]-1-propanesulfonate; Fα_{i1}, fluorescein-labeled Gα_{i1}.

10.1021/bi050655i CCC: $30.25
Published on Web 07/16/2005

the energetics of protein−protein interactions. Such areas are often targeted in naive random-peptide phage display screens because of these unique properties (reviewed in refs *11* and *12*). Some of the phage display-derived peptides had significant homology to known G$\beta\gamma$ targets such as phospholipase C (PLC) β2 (*13*). A synthetic peptide, SIRK, derived from one of the selected phage, blocked G$\beta\gamma$-dependent regulation of PLCβ2 and phosphatidylinositol 3-kinase (PI3K), yet had no effect on regulation of adenylyl cyclase (AC) type I or N-type Ca^{2+} channels, thus reinforcing the notion that G$\beta\gamma$ target molecules have both common and unique interaction surfaces (*10*).

Even though SIRK blocked G$\beta\gamma$ function in vitro, cell-permeable variants of SIRK were found to activate extracellular regulated kinase (ERK) 1/2 in various cell types through a G$\beta\gamma$-dependent mechanism (*14*). In vitro experiments revealed that SIRK facilitated nucleotide exchange-independent heterotrimer dissociation (*14*, *15*), potentially explaining the activation of ERK in intact cells: SIRK binds to G$\beta\gamma$ and releases Gα·GDP, yet by virtue of its selectivity as an inhibitor, leaves a surface of G$\beta\gamma$ available to activate the ERK pathway. However, other G$\beta\gamma$ binding peptides, including QEHA derived from AC II (*16*, *17*), and amino acids 643−670 from the C-terminal region of βARK (GRK2) (*18*), do not promote dissociation of the heterotrimer although they compete with G$\beta\gamma$ for Gα binding (*15*). This observation indicates that simple competition for Gα−G$\beta\gamma$ subunit binding is not sufficient for peptides to accelerate dissociation of Gα·GDP from G$\beta\gamma$.

To fully understand the nature of the proposed G$\beta\gamma$ hot spot, the mechanism for pharmacological selectivity of the peptides that bind to that site, and the mechanism for peptide-mediated, nucleotide exchange-independent activation of G protein signaling, it became critical to describe the peptide interaction surface on G$\beta\gamma$ in atomic detail. Here we report the crystal structure of G$\beta_1\gamma_2$ bound to an analogue of SIRK at a resolution of 2.7 Å. The structure shows that the peptide is a structural mimic of the switch II region of the G protein α subunit and occupies a site on Gβ_1 that is used by several G$\beta\gamma$ binding proteins (G$\beta\gamma$ targets). The data demonstrate that the switch II binding surface on Gβ has unique binding properties that allow for multiple target recognition, yet can be manipulated pharmacologically to achieve selective disruption of G$\beta\gamma$-dependent target recognition and G protein activation. This has important implications for therapeutic targeting of G$\beta\gamma$-dependent processes.

EXPERIMENTAL PROCEDURES

Materials. Peptides were purchased from Alpha Diagnostic International (San Antonio, TX) or Sigma-Genosys (St. Louis, MO) or synthesized by the Protein Chemistry Technology Center at UTSWMC. Peptides were HPLC purified to greater than 90% and masses confirmed by mass spectroscopy. Ni-NTA agarose was from Qiagen (Valencia, CA). Streptavidin-coated polystyrene beads were from Spherotec (Libertyville, IL). HRP-conjugated anti-M13 antibody was from Amersham Biosciences (Piscataway, NJ). HRP-conjugated neutravidin was from Pierce (Rockford, IL). All molecular biology reagents were from Invitrogen (Carlsbad, CA) unless otherwise stated. Baculovirus encoding G protein $(His)_6$-α_{i1} and γ_2 and N-terminally $(His)_6$-tagged γ_2 subunits were obtained from the laboratory of Dr. Alfred Gilman.

Derivation of SIGK. Using a doping mutagenesis and rescreening strategy, a peptide similar to the SIRK peptide was derived that had higher affinity for G$\beta_1\gamma_2$. The sequence of this peptide is SIGKAFKILGYPDYD (SIGK). In vitro studies with the SIGK peptide indicate that it too can displace Gα_{i1} from a heterotrimeric complex and also effectively prevents heterotrimer formation (*15*). This peptide was used for cocrystallization with G$\beta_1\gamma_2$.

Expression and Purification of G$\beta_1\gamma_2$ for Crystallography. High 5 cells (Invitrogen; 2×10^6 cells/mL) were infected with high titer Gβ_1 and Gγ_2 baculoviruses. G$\beta_1\gamma_2$ was purified according to Kozaza and Gilman (*19*), with modifications. All steps were carried out at 4 °C. Cells were harvested 60 h postinfection by centrifugation at 2600*g* and then resuspended in 50 mL of lysis buffer (20 mM HEPES, pH 8, 150 mM NaCl, 5 mM β-ME, 1 mM EDTA, 1 mL of Sigma protease inhibitor cocktail P-2714) per liter of cell culture. Cells were lysed by sonication and centrifuged at 2600*g* to pellet the membranes. Resuspension and homogenization of membranes were accomplished by douncing in 100 mL of lysis buffer. The membranes were solubilized by adding 1% Lubrol ($C_{12}E_{10}$; Sigma) with stirring, and the resultant solution was clarified by ultracentrifugation at 125000*g*. The supernatant was loaded onto Ni-NTA agarose (Qiagen) equilibrated with lysis buffer + 1% Lubrol. The column was washed and the Lubrol exchanged for sodium cholate using buffers Ni-A (20 mM HEPES, pH 8, 0.4 M NaCl, 5 mM β-ME, 0.5% Lubrol, 0.15% cholate) and Ni-B (20 mM HEPES, pH 8, 0.1 M NaCl, 5 mM β-ME, 0.25% Lubrol, 0.3% cholate). G$\beta_1\gamma_2$ eluted in Ni-C (20 mM HEPES, pH 8, 0.01 M NaCl, 5 mM β-ME, 1% cholate, 200 mM imidazole). The eluate was loaded onto a HiTrap Q (Amersham Biosciences) column preequilibrated with QA (20 mM HEPES, pH 8, 5 mM β-ME, 0.7% CHAPS, 1 mM EDTA). G$\beta_1\gamma_2$ was eluted in a gradient using QB (QA + 1 M NaCl). Fractions containing G$\beta_1\gamma_2$ were analyzed by SDS−PAGE and pooled. Gel filtration was performed using a tandem Sephadex 75:Sephadex 200 column (Amersham Biosciences) equilibrated with buffer GF + CHAPS (20 mM HEPES, pH 8, 150 mM NaCl, 10 mM β-ME, 1 mM EDTA, 0.7% CHAPS). The purified yield was typically 1 mg of G$\beta_1\gamma_2$/L of cell culture.

Crystallography and Data Collection. SIGK peptide was added to G$\beta_1\gamma_2$ in 1.5 molar excess, and the G$\beta_1\gamma_2$·SIGK complex was used at 7 mg mL^{-1} for crystallization. Crystals were grown by vapor diffusion using equal volumes (2 μL) of protein and reservoir solution (15−17% PEG 4000, 100 mM HEPES, pH 7.5, 0.01−0.05 M sodium acetate, 10% glycerol) at 20 °C. Crystals attained dimensions of 150 μm × 50 μm × 20 μm within 1 week. Crystals were cryoprotected in 15% glycerol and frozen in liquid nitrogen.

Native crystals of G$\beta_1\gamma_2$·SIGK were screened at Advanced Light Source (ALS) beamlines 8.2.1 and 8.2.2 (Berkeley, CA) and at the Advanced Photon Source (APS) beamline BM-19 (Chicago, IL). A data set from ALS 8.2.2 was used to determine the structure. Over 100 crystals were screened; diffraction limits varied from 7 Å to the 2.7 Å data set used for structure determination. Diffraction data were indexed, integrated, and scaled using the software package HKL2000 (*20*) (Table 1). The space group of the crystals is $P2_12_12_1$.

Table 1: Data Collection and Refinement Statistics

Data Collection	
space group	$P2_12_12_1$
unit cell	
a (Å)	45.468
b (Å)	74.669
c (Å)	108.023
α (deg)	90
β (deg)	90
γ (deg)	90
D_{min} (Å)	2.7
unique reflections	9729
redundancy[a]	3.5 (1.8)
completeness (%)[a]	90.1 (56.2)
$\langle I/\sigma \rangle$[a]	13.5 (1.6)
R_{sym}[a,b]	8.7 (41.4)
mosaicity (deg)	2.3
Wilson *B* factor (Å^2)	61.8
Refinement	
resolution (Å)	45.4−2.7
no. of atoms[c]	
protein	3058
water	37
R_{work} (%)[d]	22.7
R_{free} (%)[e]	28.7
rms deviations	
bond lengths (Å)	0.006
bond angles (deg)	1.3
rms *B* factors (Å^2)	
bonded main chain	1.29
bonded side chain	1.81
average *B* factor (Å^2)[f]	46.3

[a] Numbers in parentheses correspond to the highest resolution shell, 2.8−2.7 Å. [b] $R_{sym} = \sum_h\sum_i|I_i(h) - \langle I(h)\rangle|/\sum_h\sum_i I_i(h)$, where $I_i(h)$ and $\langle I(h)\rangle$ are the *i*th and mean measurement of the intensity of reflection *h*, respectively. [c] The final model contains residues 2−340 of Gβ_1 (of 340), 7−52 of Gγ_2 (of 68), and 1−13 of SIGK (of 15). [d] $R_{work} = \sum_h||F_o(h)| - |F_c(h)||/\sum_h|F_o(h)|$, where $F_o(h)$ and $F_c(h)$ are the observed and calculated structure factors, respectively. An I/σ cutoff was not used in the final calculations of *R*-factors. [e] R_{free} is the *R*-factor obtained for a test set of reflections consisting of a randomly selected 8% of the data. [f] *B* factors at the N-termini, including Gβ_1 residues 2−41 and Gγ_2 residues 7−13, are greater than 80 Å^2.

Phasing and Refinement. The structure of the G$\beta_1\gamma_2$·SIGK complex was solved by the molecular replacement method using the program PHASER (*21*, *22*). The coordinates of G$\beta_1\gamma_2$ in the G$\beta_1\gamma_2$·GRK2 complex (1OMW, 100% sequence identity) were used as the search model. After rigid body refinement using the maximum likelihood minimization target in CNS version 1.1 (*23*, *24*), the model was further refined by using a combination of simulated annealing, Powell minimization, and *B* factor refinement. The σA-weighted $2F_o - F_c$ electron density map computed with refined phases revealed clear main chain density for 10 residues of the SIGK peptide along with identifiable side chain density for several SIGK residues. Subsequent model building was performed in O (*25*) followed by simulated annealing, energy minimization, and *B* factor refinement using CNS. PROCHECK (*26*) analysis indicates that all residues exhibit main chain conformations in the most favored or additionally allowed regions of ϕ,ψ space (Table 1). Calculations of surface accessibility, G$\beta_1\gamma_2$·SIGK contacts, and rmsd between structures were carried out using programs in the CNS suite. Figures were generated using PyMOL (http://www.pymol.org).

Construction and Purification of Biotinylated βγ Subunits. All Gβ_1 mutants were made in the baculovirus vector PDW 464 which encodes a biotin acceptor peptide in frame with the amino terminus of Gβ_1 (*14*). All mutants were generated by overlap extension PCR using standard protocols. Baculoviruses were generated via the Bac-to-Bac system following the manufacturer's instructions (Gibco). Two hundred milliliter cultures of Sf-9 cells were triply infected with baculovirus encoding G protein $(His)_6$-α_{i1}, γ_2 and wild type or mutated bGβ_1 subunits. Sf-9 cells were harvested 60 h postinfection. Cells were lysed in 4 mL of lysis buffer (50 mM HEPES, pH 8.0, 3 mM $MgCl_2$, 10 mM *β*-mercaptoethanol, 1 mM EDTA, 100 mM NaCl, 10 μM GDP, and protease inhibitors) by freeze−thawing in liquid nitrogen. Membranes were harvested by centrifugation at 100000*g* for 20 min. The membrane pellet was suspended, incubated, and stirred with 4 mL of extraction buffer (50 mM HEPES, pH 8.0, 3 mM $MgCl_2$, 50 mM NaCl, 10 mM *β*-mercaptoethanol, 10 μM GDP, 1% cholate, and protease inhibitors) at 4 °C for 1 h. Detergent extracts were clarified by centrifugation at 100000*g* for 20 min. The supernatant was diluted 5-fold with buffer A (50 mM HEPES, pH 8.0, 3 mM $MgCl_2$, 10 mM *β*-mercaptoethanol, 100 mM NaCl, 10 μM GDP, 0.5% $C_{12}E_{10}$, and protease inhibitors), and 400 μL of Ni-NTA agarose resin was added and mixed at 4 °C for 1 h. The agarose beads were pelleted by centrifugation and washed three times with 1 mL of buffer A + 300 mM NaCl and 5 mM imidazole. G$\beta_1\gamma_2$ subunits were eluted from bound $(His)_6$-Gα_{i1} by mixing the beads in 1 mL of elution buffer (buffer A + 150 mM NaCl, 5 mM imidazole, 50 mM $MgCl_2$, 10 mM NaF, 10 μM $AlCl_3$, and 1% cholate instead of $C_{12}E_{10}$) at room temperature for 1 h. Concentrations of eluted bG$\beta_1\gamma_2$ dimers were determined by comparing to a standard curve of fully purified 100% biotinylated G$\beta_1\gamma_2$. Proteins were separated by SDS−PAGE, transferred to nitrocellulose, and probed with HRP−neutravidin (Pierce). Membranes were exposed to chemiluminescence reagents, and chemiluminescence was measured using an Epi-Chem II Darkroom system from UVP Bioimaging Systems.

Phage ELISA. Phage used in this study were from the random-peptide phage display screen described in Scott et al. (*10*) and propagated as in ref *27*. For ELISA, 1 μg of streptavidin was immobilized in the well of a 96-well plate overnight at 4 °C. The wells were blocked with 100 μL of 2% BSA in TBS for 1 h at 4 °C followed by three washes of 1× TBS + 0.5% Tween. Forty microliters of 25 nM bG$\beta_1\gamma_2$ in TBS + 0.5% Tween was added to each well and incubated at 4 °C for 1.5 h. The wells were washed, followed by the addition of 1×10^{10} phage particles and incubation at 4 °C for 3 h. The wells were then washed six times with TBS + 0.5% Tween, followed by the addition of 40 μL of a 1:5000 dilution of anti-M13 antibody (Pharmacia), and incubated at room temperature for 1 h. The wells were washed, followed by the addition of 40 μL of 2,2′-azinobis-(3-ethylbenzothiazoline)-6-sulfonic acid (ABTS), and the colorimetric reaction was monitored at 405 nm. Nonspecific binding was subtracted for each reading, and the amount of binding to each mutant bG$\beta_1\gamma_2$ subunit was expressed as a percent of phage binding to wild-type bG$\beta_1\gamma_2$.

Measurement of Gα$_{i1}$−β$_1\gamma_2$ Competition and Dissociation Kinetics by Flow Cytometry. The fluorescein-labeled Gα_{i1} (Fα_{i1}) used in these experiments was prepared as described (*28*). Two different types of assays were used to determine peptide effects on Gα−G$\beta\gamma$ interactions: competition and

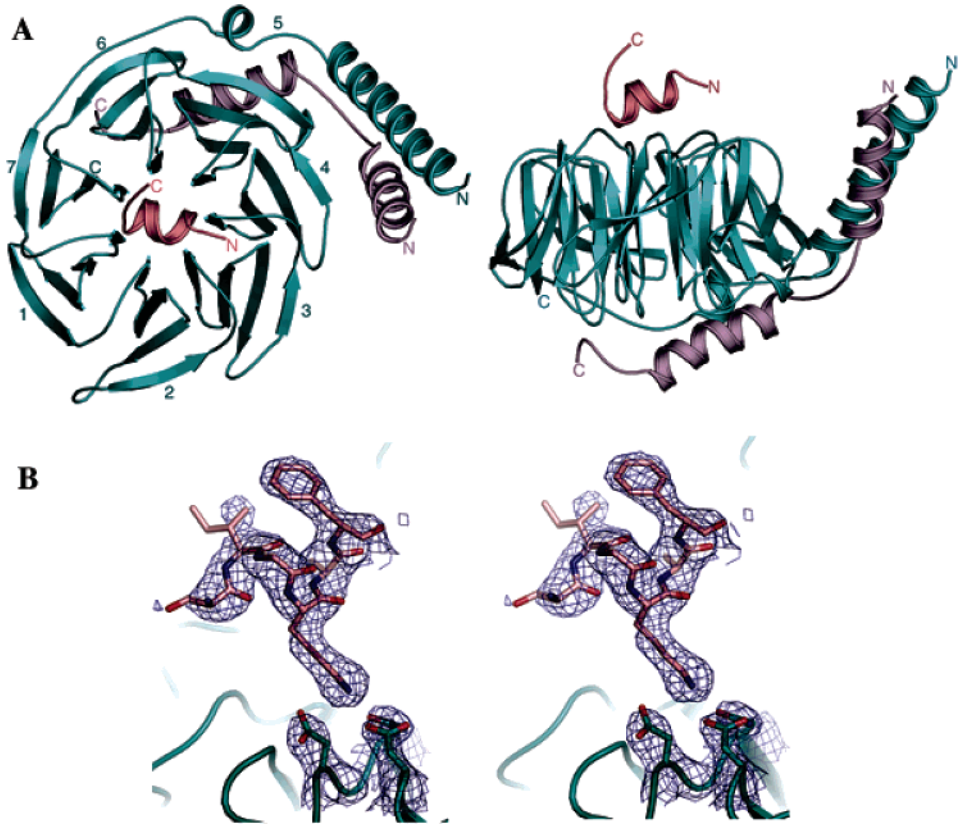

FIGURE 1: Structure of the peptide SIGK bound to the $G\beta_1\gamma_2$ heterodimer. (A) Two views of the $G\beta\gamma$·SIGK complex, shown in ribbon representation. The two representations are related by −90°. SIGK is colored pink, $G\beta_1$, blue, and $G\gamma_2$ purple. The N- and C-termini of SIGK, $G\beta_1$, and $G\gamma_2$ are labeled. On the left panel, the seven blades of $G\beta_1$ are labeled following the convention of Wall et al. (*30*, *40*). (B) Stereoview of representative σA-weighted annealed $2F_o - F_c$ electron density, contoured at 1σ. The region shown is centered on the peptide N-terminal binding site. SIGK peptide is shown in pink and $G\beta_1$ in blue.

dissociation studies which were described in detail in Ghosh et al. (*15*). Briefly, for competition-based assays 100 pM $F\alpha_{i1}$ and indicated concentrations of peptides were added to 50 pM $bG\beta_1\gamma_2$ immobilized on 10^5 beads per milliliter and incubated at room temperature for 30 min to reach equilibrium. The bead-associated fluorescence was then recorded in a BD Biosciences FACs Calibur flow cytometer. The data were corrected for background fluorescence and fit with a sigmoid dose response curve using Graph Pad Prism 4. To measure dissociation of $F\alpha_{i1}$ from $bG\beta_1\gamma_2$, 100 pM $F\alpha_{i1}$ was incubated with 50 pM immobilized $bG\beta_1\gamma_2$ at room temperature for 15−20 min. The fluorescence of the bound $F\alpha_{i1}$ subunit was measured, followed by the addition of a 200-fold excess of unlabeled $G\alpha_{i1}$ or peptides at the indicated concentrations, and the amount of $F\alpha_{i1}$ remaining bound to the beads was measured at the indicated times.

RESULTS

Architecture of the $G\beta_1\gamma_2$·SIGK Complex. As has been described previously (*29*, *30*), $G\beta_1$ is a β-propeller composed of seven four-stranded β-sheets ("blades") and an N-terminal extended helix that interacts extensively with $G\gamma_2$ (Figure 1A). Each sheet is composed of WD-40 repeats connected by loops of variable length. Residues 2−340 are included in the model. *B* factors throughout the core of $G\beta_1$ are less than 40 Å^2. Residues with *B* factors >60 Å^2 are found in three loop regions: Lys127−Ser136 in blade 2, Arg214−Met217 in blade 4, and Ser265−Ile269 in the loop connecting blades 6 and 7. $G\gamma_2$ forms a helix with a kink made by residues Asn24−Lys29 and a coil region beginning at residue His44 (Figure 1A). The average *B* factor within the $G\gamma_2$ molecule is 44 Å^2. No electron density is observed for the N-terminal 7 residues and the C-terminal 16 residues of $G\gamma_2$ or the prenyl lipid modification at the C-terminus of $G\gamma_2$.

SIGK forms an α-helical structure broken by a glycine residue at position 10 (Figure 1A). The C-terminal three residues form an extended structure that stretches away from the $G\beta_1$ molecule and is supported by crystal contacts between sPro12[2] and sAsp13 with Thr47 and Lys337 from a symmetry-related $G\beta_1$ molecule. The *B* factors for the N- (sSer1, sIle2) and C-terminal (sGly10−sAsp13) residues of SIGK are greater than 50 Å^2; those for all other residues are between 30 and 50 Å^2. The electron density for the main chain atoms in residues 1−13 are well-defined (Figure 1B); three of the SIGK side chains that do not contact $G\beta_1$ (sIle2, sLys7, and sAsp13) are disordered. The peptide binds across the "top" face of $G\beta_1$ (Figure 1A) and buries 970 Å^2 total solvent-accessible surface area. The peptide makes no contact with the $G\gamma_2$ subunit, which is bound to the "bottom" surface of the $G\beta_1$ torus.

SIGK Binds to Two Surfaces on $G\beta_1$ and Mimics the Switch II Helix of Gα. The SIGK contact surface on $G\beta_1$ is very similar to that occupied by the switch II region of Gα. This is somewhat surprising given that this surface is thought to be important for recognition of most $G\beta\gamma$ targets, yet the

[2] In the following text, amino acid identifiers prefixed with "s" refer to SIGK residues.

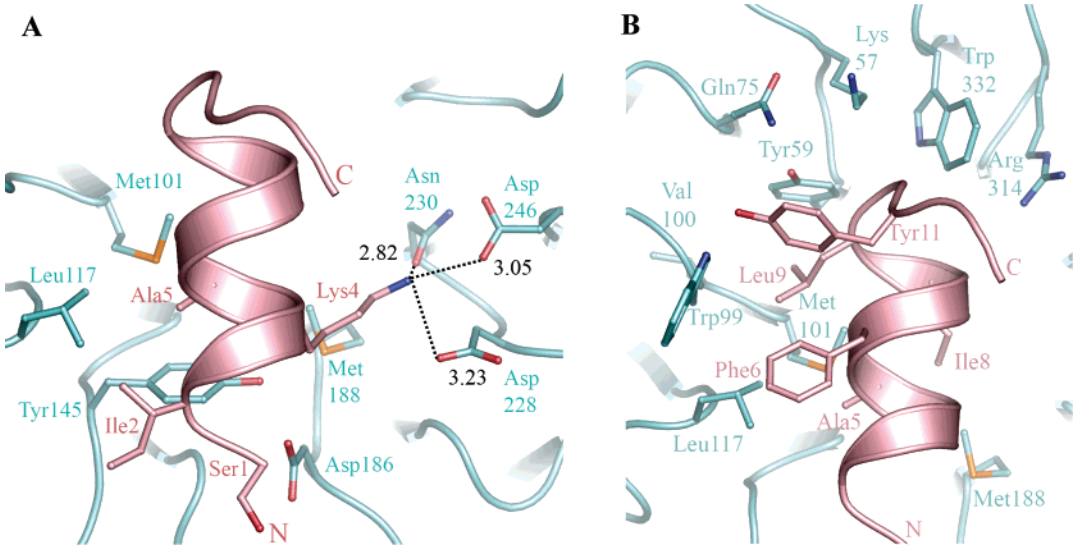

FIGURE 2: SIGK interface with Gβ_1. (A) sLys4 of SIGK (pink) points into a highly acidic pocket on Gβ_1 (teal) centered on Asp228, Asn230, and Asp246 of Gβ_1. Oxygen, nitrogen, and sulfur atoms are colored red, blue, and orange, respectively. Distances in angstroms between the Cϵ of sLys4 and the Oδ2 and Nδ2 atoms of Asp228, Asn230, and Asp246 are shown. (B) Residues sAla5−sTyr11 from SIGK (pink) form an extensive interface with the mainly hydrophobic top surface of Gβ_1 (teal). Note that Met188 and Met101 are also involved in the N-terminal interface and are shown in (A).

SIGK peptide selectively inhibits G$\beta\gamma$-dependent regulation of effectors. The binding site can be separated into two regions: an acidic region on Gβ_1 that interacts with the N-terminus of the peptide (the N-terminal site) and a largely nonpolar region that interacts with the C-terminus of the peptide (the C-terminal site). In total, 13 Gβ_1 residues directly contact SIGK, contributed by six of the seven blades of the β-propeller (Figures 2 and 3 and Supporting Information Table 1).

The N-terminal binding site is centered on an electrostatic interaction in which sLys4 projects into a negatively charged binding pocket on Gβ_1 where it forms hydrogen-bonded or charge interactions with Asp228, Asn230, and Asp246 (Figure 2A). Met188, Asp186, and Tyr145 also form multiple interactions with SIGK N-terminal residues as shown in Figures 2A and 3. The C-terminal residues of SIGK (sAla5−sGly11) pack against a largely hydrophobic pocket on Gβ_1 (Figure 2B) extending 11 Å from Trp332 on blade 7 to Met188 in blade 2. The interactions between Gβ_1 and the N-terminal and C-terminal regions of SIGK are outlined in detail in Figure 3.

Functional Analysis of the Requirements for SIGK Binding to Gβ_1. To assess the contribution of each Gβ_1 amino acid residue in the SIGK binding site toward the total binding energy, Gβ_1 residues within 4 Å of the peptide binding site were individually mutated to alanine. Asp246 was changed to Ser, since an alanine substitution resulted in misfolded protein. Asp228 could not be analyzed since substitution at this site produced only misfolded protein. An ELISA assay was used to measure the affinity of phage displaying the SIGK peptide for heterodimers containing mutant Gβ_1 (Figure 4A). Peptide binding was further assessed by measuring dose-dependent inhibition by SIGK of heterotrimer formation between Gα_{i1} and G$\beta_1\gamma_2$ heterodimers formed with mutant Gβ_1 (Figure 4B). Two-thirds of the Gβ_1 mutants were tested in the assay (data not shown), and a strong correlation between binding in the phage ELISA and the IC_{50} for peptide competition with heterotrimer formation was established. Figure 4B shows representative dose response curves for some of the Gβ_1 mutants spanning a wide range of affinities for SIGK peptide. None of the mutations had substantial effects on either steady-state heterotrimer formation or heterotrimer dissociation (Supporting Information Table 2).

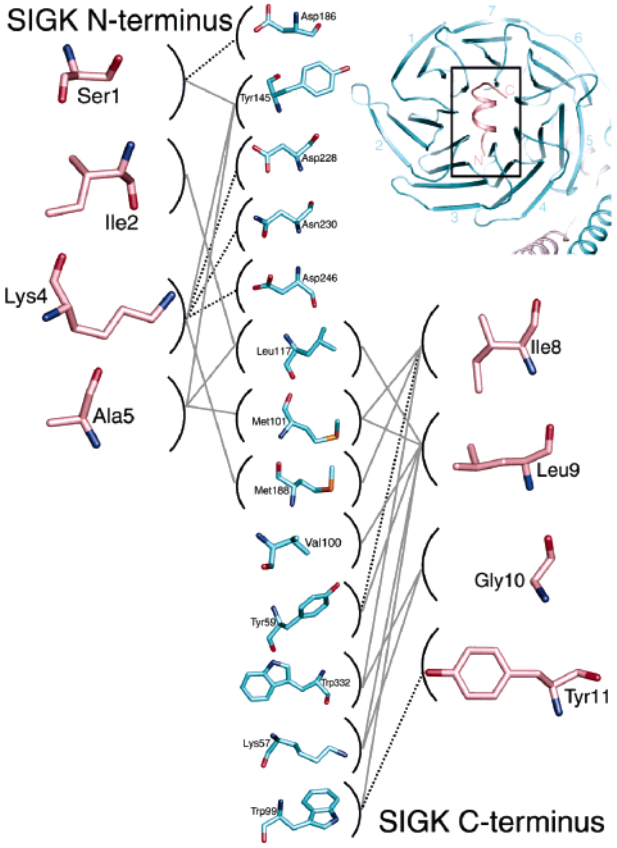

FIGURE 3: Graphical representation of the contacts between Gβ_1 and SIGK peptide. Residues from Gβ_1 are shown in blue in the middle column, flanked on the right and left columns by C- and N-terminal residues from the SIGK peptide, respectively. Polar contacts are represented by black dashed lines; nonpolar interactions are shown in gray unbroken lines.

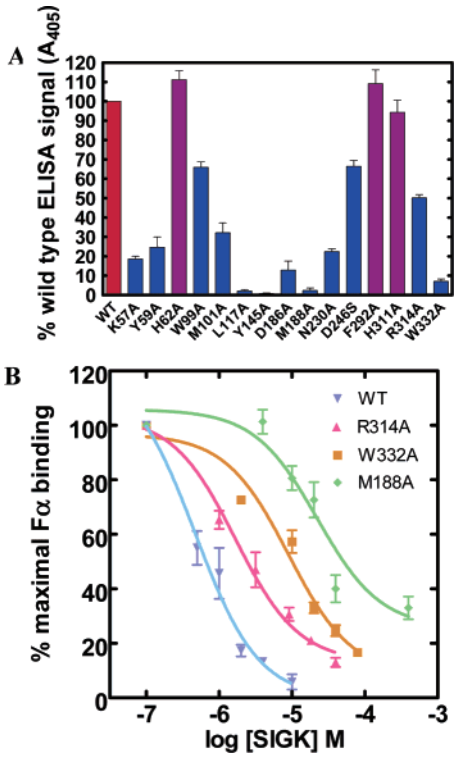

FIGURE 4: Binding of SIGK peptide to $G\beta_1\gamma_2$ mutants. (A) Amino acids that contact the SIGK peptide were individually mutated to alanine, and binding to peptide was assayed using a phage ELISA. Immobilized $bG\beta_1\gamma_2$ was incubated with phage displaying SIGK peptide. Phage binding was detected using an α-phage antibody; the raw data are absorbance at 405 nm. Data shown are the mean ± SD of triplicate determinations from three independent experiments. Blue bars represent mutants for which binding is statistically different from wild type ($p < 0.001$ as determined by a one-way ANOVA followed by a Bonferroni's post test). Purple bars represent data statistically identical to wild type. (B) SIGK competition for FITC-$G\alpha_{i1}\beta_1\gamma_2$ interactions with representative $G\beta_1$ subunit mutants. SIGK and FITC-α_i were simultaneously added to streptavidin beads coated with wild-type or mutant $bG\beta_1\gamma_2$ protein, and the amount of FITCα_{i1} bound to the beads was assayed by flow cytometry. Data are shown as the mean of triplicate determinants ± standard deviation of a representative experiment. The experiment was repeated two (Met188A) or three (wild type, Arg314A, Trp332A) times with similar results. Comparison of the two assays over a selection of mutants that spanned the range of SIGK binding affinities indicates that a 50% loss of binding translates into a 5-fold increase in IC_{50}, a 75% loss of binding corresponds to a 10-fold increase, a 90% loss is a 20-fold shift, and a 98% loss is a 50-fold shift. The IC_{50} values are as follows: wild type = 0.47 μM, Arg314A = 1.5 μM, Trp332A = 9 μM, and Met188A = 22 μM.

The structural and mutagenic data for binding of SIGK to $G\beta_1$ are graphically summarized in Figure 5. Within the N-terminal site, mutations to amino acids Tyr145 and Met188 nearly abolished binding of SIGK to $G\beta_1$ (Figure 4A). Met188 contacts sLys4 in the N-terminus as well as sIle8 near the C-terminal interface (Figure 2), and its substantial contribution to binding affinity could be attributed to contacts with both ends of the peptide. Interestingly, mutation of Asp246 had little effect on binding, even though it is involved in a polar interaction with sLys4 (Figure 4A). sLys4 is also involved in polar interactions with both Asn230 and Asp228, which may compensate for a loss of binding at Asp246 (Figure 2A). Mutation of Asn230 produces a much greater loss of binding than Asp246Ser (Figure 4A).

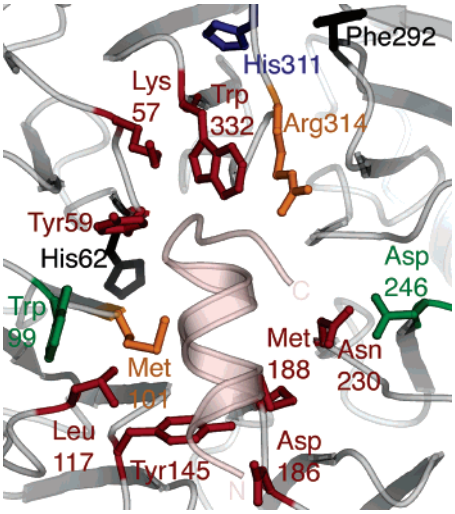

FIGURE 5: Analysis of binding of SIGK to $G\beta\gamma$. Residues mutated in the present study are shown in relation to the SIGK peptide. The N- and C-termini of the SIGK peptide (pink) are labeled. Residues of $G\beta_1$ that, when mutated to alanine, result in 75−100% loss in affinity for SIGK are colored red; a 50−75% loss, orange; a 25−50% loss, green; a 0−25% loss, blue; no effect, black. The Asp246 mutation is to serine, not alanine.

At the C-terminal binding site, mutation of Trp332 and Leu117 produces the most substantial losses of binding to SIGK, with significant effects also seen when mutations to Lys57 and Tyr59 are made (Figure 4A). All four of these amino acids are involved in multiple contacts with peptide residues, of which the majority are mediated through residues sIle8 and sLeu9 (Figure 3 and Supporting Information Table 1). The data indicate that the interactions of sIle8 and sLeu9 with other residues in $G\beta_1$ (for example, Leu177 and Met188) contribute more to SIGK binding than Trp99, whose mutation had little effect on peptide binding (Figure 4A). Overall, these data support the structural model, but there are some surprises where amino acids predicted to be important based on the structural information actually contribute little to the binding interaction (W99, for example).

Nature of Molecular Recognition by a Preferred Protein Interaction Surface. The phage display screen against $G\beta_1\gamma_2$ identified many peptides of differing amino acid sequence that all bound to a surface that overlaps the SIGK binding site (*10*). To understand how $G\beta\gamma$ recognizes a diverse array of amino acid sequences at a single binding site, we tested binding of the alanine-substituted $G\beta_1$ mutants (and the Asp246Ser mutant) to phage displaying each of nine different peptides from the original phage display screen (Table 2). The nine peptides were chosen to represent the four different consensus groups of peptides identified previously (see ref *10* and Table 2). Binding of phage displaying these peptides to wild-type $G\beta_1\gamma_2$ gave ELISA signals that were different but fell within a similar range (Figure 6A). Any substitution that decreased binding to less than 20% of wild type was considered to be a critical binding contact for that peptide.

The data in Figure 6B are sorted by consensus group. The data show that each group utilizes a characteristic combination of $G\beta_1$ residues within the SIGK interaction surface to achieve binding. Within groups I and II, there are substantial differences between the sets of strong $G\beta\gamma$ binding determinants. A dominant feature among all of the peptides is a

Table 2: Peptides Used in This Study

Phage Name	Sequence[a]	
3.14	SIG**K**AFK**ILG**YPDYD	
2F	LCS**K**AYL**LLG**QTC	**GROUP I**
C1	SCKRT**K**AQI**LLA**PCT	
C14	WCPP**K**AMT**QLG**IKAC	**GROUP II**
3C	SCGHGL**K**VQS**TIG**ACA	
C4	SCEKR**YGI**EFCT	
C5	SCEKR**LGV**RSCT	**GROUP III**
C8	SCAR**FFG**TPGCT	
C2	WCPP**K**LEQ**WYD**GCA	**GROUP IV**

[a] Shown in bold is the lysine residue contacting the N-terminus in SIGK and the analogous lysine and hydrophobic core residues in the other peptide families. Peptides were grouped into families on the basis of the internal sequence homology identified in ref *10*.

strong requirement for Trp332 within the C-terminal binding site. Lys57, Tyr59, and Leu117, also within this site, contribute significantly although they are not absolutely required for binding of certain peptides in groups II and III. Mutation of the remainder of the amino acids had more variable effects on binding of each peptide. For example, SIGK has a minimal requirement for Trp99 while SCKRTKAQILLAPCT absolutely requires Trp99 for binding. The reverse is true for Tyr145 where SIGK binding has an absolute requirement for Tyr145 and SCKRTKAQILLAPCT binding is not affected by this mutation.

In general, peptides in groups I, II, and IV have a substantial requirement for binding to the N-terminal binding surface as reflected by an almost complete loss of binding to the Met188Ala and Asp246Ser mutants and the requirement of various peptides for Asn230 (Figure 6B). The peptides in group I have a conserved motif in which a lysine is spaced three amino acids away from a hydrophobic core motif (see Table 2). This motif in SIGK provides the appropriate spacing in a single α-helical turn between the sLys4 that interacts with the N-terminal binding surface and the ILG motif that interacts with the C-terminal site (Figure 2). Peptides in groups II and IV show a similar motif with a spacing of four residues. The peptides in group III bind the C-terminal site but lack a requirement for Met188 and have minimal requirements for Asn230 and Asp246, suggesting that they do not rely on the N-terminal binding surface for their interaction with Gβ_1 (Figure 6B). Interestingly, some of the mutations actually appear to increase binding of a group IV peptide, but the mechanism for this is unclear.

Mutant Gβ_1 proteins containing substitutions at either of two amino acids, Arg314 and His311, which do not bind directly to SIGK were also analyzed (Figure 5). His311 and Arg314 were mutated because they undergo a conformation change in G$\beta_1\gamma_1$ heterodimers upon binding of phosducin (*31*, *32*). It is unlikely that His311 directly interacts with amino acids from any of the phage display derived peptides; nevertheless, mutation of His311 to alanine affected binding of various peptides to differing extents (Figure 6B). Peptides whose binding was affected by His311Ala also required Arg314 for binding, and we suspect that the effect of mutating His311 to alanine could be due to an alteration in the position of Arg314.

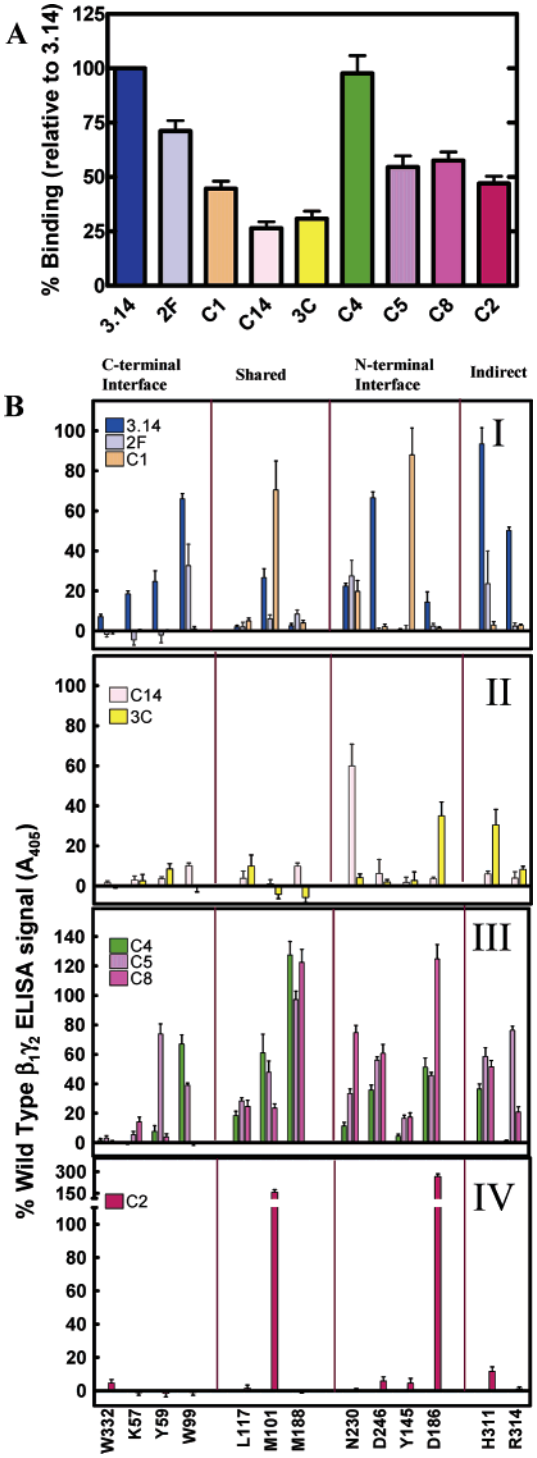

FIGURE 6: Defining the nature of peptide binding to the hot spot. (A) Relative ELISA signals of phage binding to wt G$\beta_1\gamma_2$ are shown to indicate that they all give similar binding signals. The sequences of the peptides displayed by the various phage as fusions with the coat protein are shown in Table 2. Data are shown as mean ± SD of duplicate determinations for three independent experiments. (B) ELISA based assay to assess binding of phage displaying various peptides to Gβ_1 mutants with alanine substitutions (except Asp246 which was mutated to S) at the positions shown in Figure 5. Wild-type or alanine-substituted biotinylated G$\beta_1\gamma_2$ subunits were immobilized on a streptavidin-coated 96-well plate, followed by the addition of phage. Phage binding was assessed as described in Experimental Procedures. The data are corrected for nonspecific binding of phage to the plate and are represented as a percent wild-type binding. Data shown are mean ± SD of duplicate determinations from three independent experiments.

Structural Changes in $G\beta_1$ upon Binding SIGK. We previously suggested that one mechanism to account for peptide-dependent acceleration of heterotrimer dissociation could involve a change in conformation of $G\beta\gamma$ upon peptide binding (*15*). However, the structural data indicate that the surface of $G\beta_1$ in the $G\beta_1\gamma_2$·SIGK complex is not significantly altered. The rmsd between the core residues of $G\beta_1$ in the $G\beta_1\gamma_2$·SIGK complex and that in the uncomplexed $G\beta_1\gamma_1$ heterodimer [1TBG (*29*); Val40−Asn340, Cα only] is 0.88 Å. However, the side chains of Trp99, Tyr59, Asp228, Leu117, and Met101 rotate to accommodate SIGK such that atoms within these residues undergo maximum displacements of 4.0, 3.6, 2.9, 2.8, and 2.3 Å, respectively, relative to their positions in uncomplexed $G\beta_1$. The *B* factors for residues in the SIGK binding surface are close to the overall average for the complex. However, the *B* factor for Trp99 is reduced 2-fold upon binding to SIGK, as indicated by comparison of normalized *B* factors of the respective structures. The SIGK·$G\beta_1\gamma_2$ complex was also compared to those of five $G\beta_1\gamma_2$ complexes with protein targets: the $G\beta_1\gamma_2$·$G\alpha_{i1}$ heterotrimer (1GG2) (*30*) and the $G\beta_1\gamma_1$·$G\alpha_{t/i}$ heterotrimer (1GOT) (*33*), the $G\beta_1\gamma_1$·phosducin complex (1AOR and 2TRC) (*31*, *32*), and the $G\beta_1\gamma_2$·GRK2 complex (1OMW) (*34*). Superposition of the $G\beta_1\gamma_2$·SIGK complex with each of these structures yields average rms deviations for $G\beta_1$ residues 40−340 of less than 1.0 Å (Cα only). With the exception of a few residues involved in the $G\beta_1\gamma_1$·phosducin complex, the $G\beta\gamma$ heterodimer does not undergo large-scale structural rearrangements in order to bind either the SIGK peptide or protein targets.

Amino Acid Sequence Characteristics of Peptides That Accelerate Heterotrimer Dissociation. Previously, we demonstrated that, unlike SIRK, two peptides predicted to bind at the Gα−$G\beta\gamma$ interface [the βARK-ct peptide (amino acids 643−670) and QEHA] blocked heterotrimer formation but could not promote heterotrimer dissociation (*15*). Since there is no apparent conformational change in $G\beta$ upon SIGK binding, yet SIGK has an apparently unique ability to accelerate heterotrimer dissociation, we hypothesized that specific interactions at this interface are required for peptides to promote dissociation of $G\beta\gamma$ from Gα·GDP. To explore this idea in greater depth, we examined the effects of SCAR, another peptide derived from the phage display screen, to promote subunit dissociation. Amino acids within the N-terminal interaction interface which contact sLys4 of SIGK, including Asn230, Asp246, and Met188, are not important for binding SCAR (Figure 7A). SCAR lacks a lysine residue with the correct positioning relative to the hydrophobic core motif to reach the sLys4 binding N-terminal surface (Table 2). We hypothesized that this difference in binding interaction would affect the ability to promote heterotrimer dissociation. Both SIGK and SCAR can compete with $G\alpha_{i1}$ for binding to $G\beta_1\gamma_2$ with IC_{50} values of 0.5 and 1.7 μM, respectively (Figure 7B). However, unlike the SIGK peptide, saturating concentrations of SCAR peptide do not promote dissociation of a preformed heterotrimer (Figure 7C,D). The inability of SCAR to promote heterotrimer dissociation is not due to its marginally lower binding affinity relative to SIGK, since SIRK (SIRKALNILGYPDYD), a peptide used in our original studies (*10*), has a similar affinity and promotes dissociation (see Figure 8 and ref *15*). These results support the hypothesis that peptide binding to the N-terminal interface is necessary for acceleration of heterotrimer dissociation.

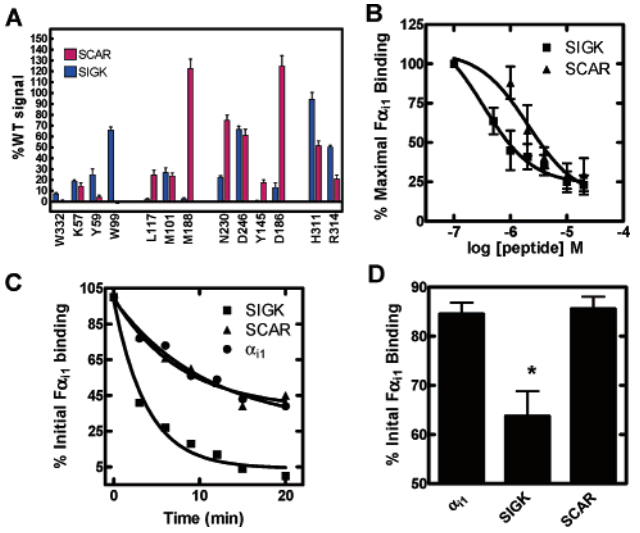

FIGURE 7: SCAR peptide competes with Gα for binding to $G\beta\gamma$ but does not promote heterotrimer dissociation. (A) Direct comparison of the amino acids required for binding to phage displaying SIGK (blue) and the SCAR peptide (red) as determined by a phage ELISA. (B) Representative dose response curves for blocking of $F\alpha_{i1}$−$G\beta_1\gamma_2$ interactions by SIGK or SCAR peptides. Data are corrected for background and are shown as mean ± SD of duplicate determinations from one experiment and are fit with a sigmoid dose response curve using Graph Pad Prism 4. The IC_{50} values are as follows: SIGK, 0.6 μM; SCAR, 1.4 μM. The experiment was repeated three times with similar results. (C) Kinetics of dissociation of a preformed $F\alpha_{i1}$−$G\beta_1\gamma_2$ heterotrimer by the addition of 25 μM SIGK, 80 μM SCAR, or excess unlabeled myristoyl-$G\alpha_{i1}$ (to measure the intrinsic dissociation rate). Data were fit with a one-phase exponential decay curve using Graph Pad Prism 4. The experiment was repeated three times with similar results. (D) Pooled data from six experiments showing the extent of heterotrimer dissociation 3 min after addition of excess myristoylated $G\alpha_{i1}$ or peptide. Data are the mean ± SD from six experiments. *: $p < 0.001$ compared to $G\alpha_{i1}$ as determined with a one-way ANOVA followed by a Bonferroni's post test.

To more directly assess the importance of specific interactions with the N-terminal binding site, a key contact to the N-terminal binding pocket of $G\beta$ was eliminated by mutating sLys4 of SIRK to alanine. SIRK(K4A) had a markedly lower IC_{50} than SIRK (IC_{50} = 60 vs 1.4 μM) for blocking Gα−$G\beta\gamma$ interactions (Figure 8A); however, at high concentrations it blocked to levels near that of SIRK (Figure 8A,B). Despite blocking Gα−$G\beta\gamma$ interactions, SIRK(K4A) failed to accelerate heterotrimer dissociation (Figure 8C,D). The apparent off-rate of $F\alpha_{i1}$ from $G\beta_1\gamma_2$ is lower in the presence of SIRK(K4A) than the intrinsic dissociation rate. This could be because SIRK(K4A) is a low-affinity blocker and is not effective at preventing rebinding of $F\alpha_{i1}$. To confirm that the inability of SIRK(K4A) to induce heterotrimer dissociation is not due to its low affinity for $G\beta_1\gamma_2$, we tested a peptide, SIRK(G10A) ($IC_{50} \sim 80$ μM), which has an affinity comparable to that of SIRK(K4A). This peptide contains a lysine residue at position 4, but alanine is substituted for glycine at position 10. Therefore, SIRK(G10A) is expected to retain binding to the N-terminal $G\beta_1$ subsite but would have reduced affinity due to the loss of interactions with the C-terminal subsite. As expected, SIRK(G10A) blocked heterotrimer formation at high concentrations (Figure 8A,B) but, despite its low affinity for $G\beta_1\gamma_2$, could still accelerate

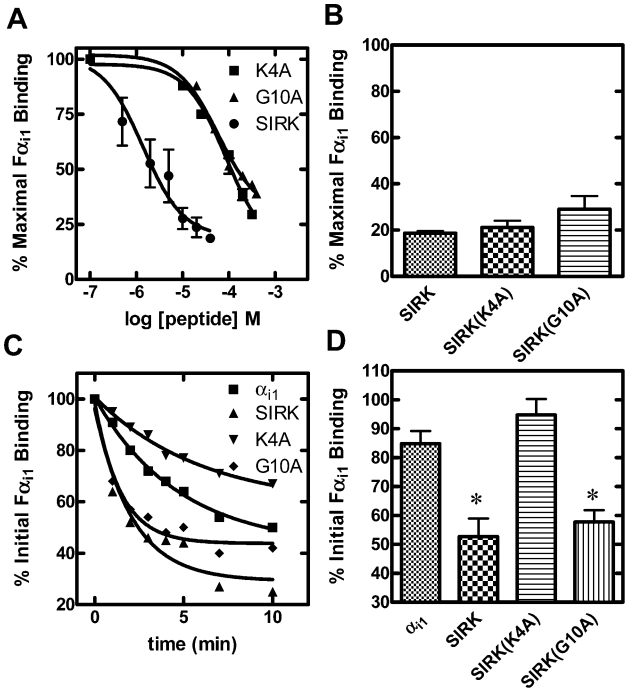

FIGURE 8: Binding of the K4 residue of SIRK is essential for peptide-mediated dissociation. (A) Competition for binding between 50 pM bG$\beta_1\gamma_2$ between 100 pM Fα_{i1} and SIRK, SIRK(K4A), or SIRK(G10A). The IC_{50} values are as follows: SIRK, 1.4 μM; SIRK(K4A), 60 μM; SIRK(G10A), 80 μM. Data are the mean ± SD from duplicate determinations from one of three independent experiments. (B) Pooled data from three experiments showing the amount of inhibition of Fα_{i1} binding with 50 μM SIRK, 300 μM SIRK(K4A), and 400 μM SIRK(G10A) in competition assays. (C) Kinetics of dissociation of a preformed Fα_{i1}−G$\beta_1\gamma_2$ heterotrimer by 50 μM SIRK, 300 μM SIRK(K4A), and 400 μM SIRK(G10A) peptides or excess unlabeled myristoyl-Gα_{i1}. Data shown were fit with a one-phase exponential decay function using Graph Pad Prism 4. The experiments were repeated four times with similar results. (D) Pooled data from four experiments showing the amount of Fα_{i1} remaining bound to bG$\beta_1\gamma_2$ 3 min after addition of peptide or excess unlabeled myristoylated Gα_{i1}. Data are shown as the mean ± SD from four independent experiments. *: $p < 0.0001$ compared to Gα_{i1} as determined with a one-way ANOVA followed by a Bonferroni's post test.

heterotrimer dissociation (Figure 8C,D). Therefore, the ability of SIRK to bind to Gβ_1 and promote heterotrimer dissociation seems to require the presence of Lys4 and its consequent ability to interact with the N-terminal subsite of Gβ_1.

DISCUSSION

It had been discovered that a group of peptides derived from a random-peptide phage display screen compete with each other for binding to G$\beta_1\gamma_2$ and, therefore, are presumed to interact at a common site (*10*). However, these peptides are selective in their ability to inhibit binding of G$\beta_1\gamma_2$ to its various interaction partners. This work demonstrates that one of these inhibitory peptides, SIGK, targets the Gα_{i1} switch II binding surface of G$\beta_1\gamma_2$, the same surface that is used by most G$\beta\gamma$ effectors and binding proteins (*5*). This explains the ability of this peptide to inhibit interactions between G$\beta\gamma$ and multiple targets, but the pharmacological selectivity of this peptide demonstrates that this binding surface is not responsible for all target recognition. Second, our mutational analysis of the binding requirements for the families of different inhibitory peptides demonstrates that the G$\beta_1\gamma_2$·SIGK interface has the capacity to bind multiple amino acid sequences. Thus the G$\beta\gamma$ binding site, which is used both by effectors and by peptides selected though phage display, is a paradigm for multiple target recognition. Third, we find that binding of peptides at the top face of Gβ_1 can promote G protein subunit dissociation and that specific binding requirements within the surface are required for this activity. Consequently, this biologically important event can be dissected pharmacologically using peptides.

The SIGK Peptide Binding Surface on Gβγ Uses Diverse Mechanisms for Amino Acid Sequence Recognition. No two peptides from the phage display screen bound to the SIGK−G$\beta_1\gamma_2$ binding surfaces using the same molecular determinants; even peptides in the same consensus group with similar sequences had unique modes of binding (Figure 6B). The multiple modes of peptide binding suggested by the mutagenesis experiments are in accordance with the way in which G$\beta\gamma$ interacts with a wide array of target molecules; G$\beta\gamma$ binding partners lack consensus sequences and geometries, although many G$\beta\gamma$ binding partners access the top face of Gβ utilizing identical residues of Gβ. For example, Lys57, Tyr59, Trp99, Met101, Leu117, Tyr145, Met188, Asp246, and Trp332 from Gβ_1 are involved in contacts with the GRK2 PH domain in the crystal structure of the G$\beta_1\gamma_2$·GRK2 complex, and all of these residues of Gβ_1 are involved in SIGK contacts as well (Figure 9 and Supporting Information Table 3). This is in spite of the fact that the secondary structures of the GRK2 PH domain (the RH−PH loop, the αCT region, and β4 strand) are completely dissimilar to the purely helical SIGK peptide (*34*). This theme is recapitulated in the complex of Gβ_1 with Gα (*30*, *33*). Notably, the switch II region of Gα_{i1} forms an α-helix that is bound in almost the same orientation as the SIGK peptide (Figure 7A). However, switch II of Gα_{i1} has no sequence similarity to the SIGK peptide, although it contains a lysine (Lys210) that is oriented in almost the same position as sLys4 (*30*). The array of peptides selected in the original phage display recapitulates many of the binding characteristics of G$\beta\gamma$ binding in the context of signaling molecules.

Analysis of the SIGK Binding Surface as a Preferential Protein Binding Site. The ability of the SIGK binding site of G$\beta_1\gamma_2$ to accommodate a range of ligands with diverse sequences and secondary structures suggests that it may be an example of a preferential protein binding site as described by Delano et al. (*11*). Preferential binding surfaces are characterized as having high solvent accessibility, low polarity, and a high degree of conformational flexibility (*11*, *12*, *35*−*37*). Moreover, preferential binding sites are likely to contain an unusually high concentration of so-called hot spot residues that, if mutated to alanine, reduce binding energy at least 10-fold (*11*). Often, point mutation of any hot spot residue on a surface completely abrogates protein−protein or small molecule complex formation, even when the binding interface buries several hundred angstroms squared of total surface area (*35*, *36*, *38*). We have used these criteria to evaluate the SIGK binding site of Gβ_1 as a protein surface that is predisposed by its chemical composition and surface properties to serve as a preferred protein binding site.

First, of the 12 residues in the SIGK contact surface that were tested in the current study, 8 (Lys57, Tyr59, Leu117, Tyr145, Asp186, Met188, Asn230, and Trp332) met the

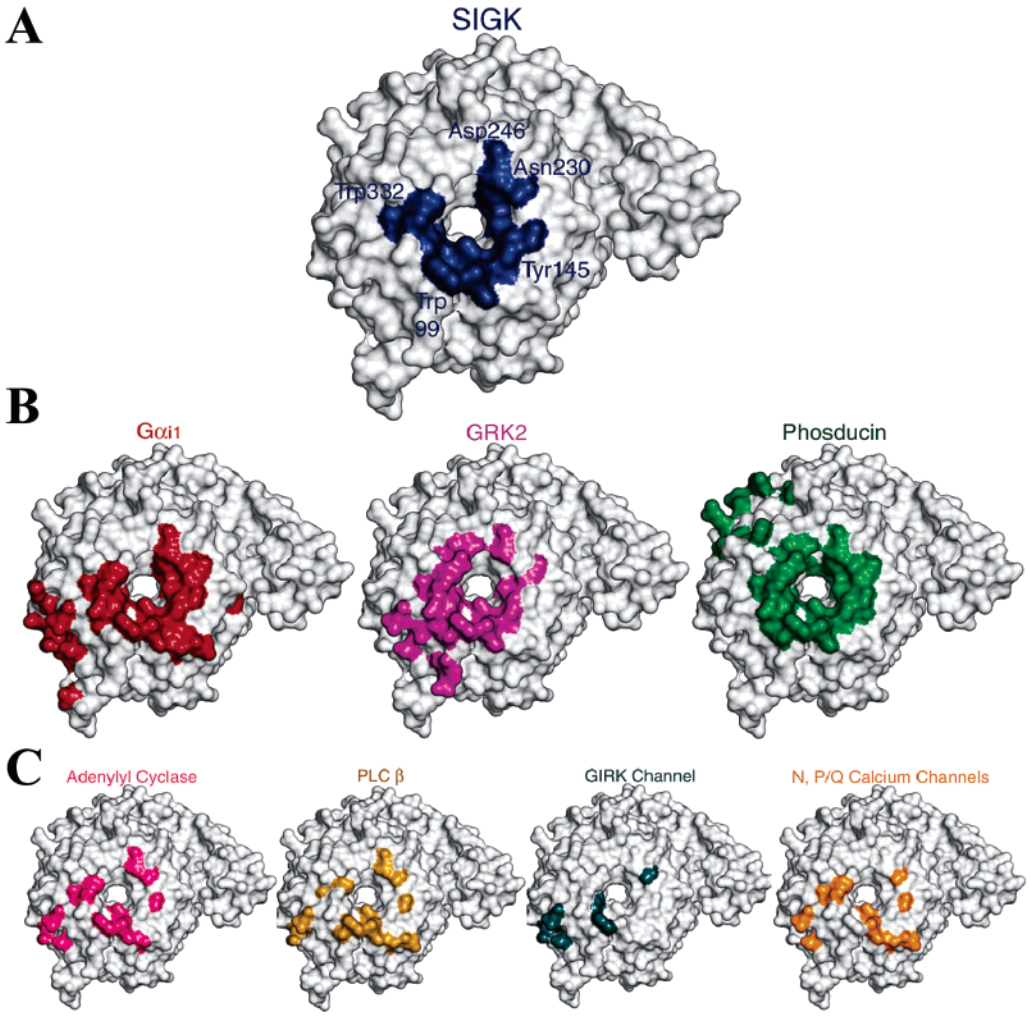

FIGURE 9: Molecular surface comparisons of G$\beta\gamma$ binding interactions. Molecular surfaces are shown for G$\beta\gamma$; the residues in each color correspond to the Gβ binding surface for each signaling target. (A) Residues that contact the SIGK peptide. Relative positions of key residues of the G$\beta_1\gamma_2$·SIGK interaction discussed in the text are labeled on the surface for orientation purposes. (B) Residues indicated by complex crystal structures to be important for target binding (*30*−*34*, *40*). (C) Residues proposed to be important for target binding to G$\beta\gamma$ based on mutagenesis studies of PLC β2, adenylyl cyclase type II, GIRK channels, and N, P/Q Ca^{2+} channels (*5*−*7*, *41*). The G$\beta\gamma$ binding partner for each molecule is labeled.

energetic criterion for a hot spot residue with respect to binding of the SIGK peptide. In addition, the SIGK binding surface is significantly more populated with aromatic residues than the rest of the Gβ surface; 38% of the SIGK binding surface versus 8.5% of the total non-glycine solvent-accessible surface of Gβ_1 is composed of Phe, Tyr, His, or Trp. In total, 62% of the SIGK binding surface is nonpolar compared to 29% of Gβ_1 solvent-accessible residues. Accessibility scores for SIGK binding residues relative to residues of the same type in Gβ_1 are shown in Supporting Information Figure 1A. Five residues within the SIGK binding surface showed significant deviation from the mean: Tyr59, Trp99, Met101, Leu117, and Trp332. Nearly one-third of the SIGK binding site residues have higher surface accessibility than would be expected for their amino acid type.

Residue flexibility can be quantified in terms of relative positional variation in the context of several G$\beta\gamma$−protein complexes as shown in Supporting Information Figure 1B. Relative to their positions in uncomplexed G$\beta_1\gamma_1$, the SIGK binding residues of Gβ_1 show only slightly greater than average side chain positional disparity (1.42 Å compared to 1.35 Å), with the side chains of Trp99, Asp228, and Trp332 having the largest positive deviation from the average (each greater than 2 Å). The largest displacements, more than 10 Å toward the outside of the Gβ_1 torus, are observed for residues Arg314 and Trp332 only in the complex with phosducin. Atomic *B* factors also provide a measure of conformational flexibility. In the structure of uncomplexed G$\beta_1\gamma_1$ the *B* factors for Trp99, Val100, and Met101 exceed the mean value by least one standard deviation (Trp99 is greater than 2 SD from the mean). In complexes with Gα_{i1}, GRK2, phosducin, and SIGK, these binding site residues become more well ordered with *B* values close to the mean and in some cases up to 1 SD below the mean (data not shown). Taken together, these two measures of conformational flexibility indicate that the Gβ_1 binding surface undergoes multiple small structural changes to accommodate structurally diverse binding partners.

In total, structural, mutagenic, and computational analysis demonstrates that the SIGK binding site on Gβ_1 may be regarded as a hot surface. In this particular case, the ability to bind diverse sequence targets appears to depend on heterogeneous nonbonded interactions; residues are utilized that use van der Waals contacts (methionine and leucine), polar contacts (aspartate and asparagine), and both (lysines,

tryptophan, and tyrosine) to contribute to the energy of binding.

Interactions with the Lysine Binding Pocket on Gβ Subunits Are Critical for Peptide-Mediated Subunit Dissociation. The crystal structure of the G$\beta_1\gamma_2$−SIGK complex clearly shows why SIGK and related peptides compete for binding with Gα; they bind to the same surface on G$\beta\gamma$ as the Gα switch II region (*30*, *33*). However, our data clearly show that SIGK and SIRK promote heterotrimer dissociation, thereby providing a novel means to effect G protein activation in vitro and in intact cells (*14*, *15*). It is not known how SIGK/SIRK catalyzes heterotrimer dissociation. Two major interfaces on Gα subunits contact Gβ: the switch interface, which overlaps with the peptide binding site, and an interface between the N-terminus of the Gα subunit and the outer strands of blade 1 [as numbered in Wall et al. (*30*)]. These surfaces may separately and transiently release from G$\beta\gamma$, with Gα subunit dissociation occurring only when both interactions are broken simultaneously. It is possible that the SIGK and SIRK peptides are able to promote dissociation in part because they bind G$\beta\gamma$ while the switch II interface is transiently accessible, followed by release of the N-terminus of the Gα subunit from G$\beta\gamma$ which leads to full subunit dissociation.

However, other peptides that can compete for Gα−G$\beta\gamma$ interactions, including βARK-ct peptide, QEHA, or SCAR, do not promote dissociation. We propose that SIRK and SIGK have the unique capacity to catalyze dissociation because they bind to the peptide N-terminal binding site on Gβ. Peptides unable to bind this region such as SCAR and SIRK(K4A) could not promote subunit dissociation, even though they compete with Gα for G$\beta\gamma$ binding. These results also demonstrate that high peptide affinity is neither necessary nor sufficient to enhance the rate of heterotrimer dissociation. SCAR, a high-affinity peptide, could not promote dissociation, whereas SIRK(G10), a very low affinity peptide, could. Perhaps the ability of certain peptides to interact with the charged pocket on Gβ imparts a kinetic advantage such that they are able to insert themselves at the switch II/G$\beta\gamma$ interface during rapid and transient intersubunit breathing transitions. Overall, the data indicate that a specific mechanism is required for these peptides to promote subunit dissociation and that simple competition for Gα−G$\beta\gamma$ interactions is not sufficient for this mechanism of G protein activation.

Pharmacological Importance. Our studies demonstrate a mechanism for molecular recognition of diverse ligands at a specific region on the Gβ subunit. We have shown that different peptide ligands interact with this surface through unique binding modes, corresponding well to the diversity of G$\beta\gamma$ interactions with its numerous binding partners (Figure 9). G$\beta\gamma$ binding partners lack consensus sequences and structures, yet all can utilize similar surfaces for activation. This interesting phenomenon has hindered attempts to target G$\beta\gamma$ therapeutically. G$\beta\gamma$ inhibitors such as βARK-ct and QEHA block G$\beta\gamma$ signaling nonspecifically, by inhibiting all G$\beta\gamma$ signaling downstream of receptor activation (*16*, *18*, *39*). However, unlike these inhibitors, the SIRK peptide is unique with regard to its functional selectivity. SIRK blocks G$\beta\gamma$ binding to Gα, promotes heterotrimer dissociation, and blocks activation of PI3K and PLCβ while having no effect on regulation of N-type Ca^{2+} channels or ACI. Here we have shown that, even within the switch II interface, selectivity can be achieved. G$\beta\gamma$ binding partners utilize unique sets of amino acids within this interface to mediate binding. Perhaps small organic molecules that target smaller areas within this interface might be even more specific inhibitors of G$\beta\gamma$ signaling that would be useful in the treatments of diseases such as heart failure and inflammation.

ACKNOWLEDGMENT

We thank the staffs of the Structural Biology Center at the Advanced Photon Source ID-19 and BM-19 lines and the HHMI beam lines at the Advanced Light Source for assistance with data collection and Dr. Z. Chen and Dr. S. Raghunathan for advice on structure determination. We also thank Nancy Ward for help with b-β mutagenesis, Dr. Mousumi Ghosh for help with the flow cytometry assay, and Dr. Richard Neubig for supplying Fα_{i1}.

SUPPORTING INFORMATION AVAILABLE

Tables 1−3 showing a description of the SIGK binding site on Gβ_1, Gα_{i1} binding to bG$\beta_1\gamma_2$ containing various mutant Gβ_1 subunits, and interaction surfaces for Gβ_1 binding partners, respectively, and Figure 1 showing hot-spot characteristics of the SIGK binding site of Gβ_1. This material is available free of charge via the Internet at http://pubs.acs.org.

REFERENCES

1. Gilman, A. G. (1987) G proteins: transducers of receptor-generated signals, *Annu. Rev. Biochem. 56*, 615−649.
2. Hamm, H. E. (1998) The many faces of G protein signaling, *J. Biol. Chem. 273*, 669−672.
3. Takesono, A., Cismowski, M. J., Ribas, C., Bernard, M., Chung, P., Hazard, S., Duzic, E., and Lanier, S. M. (1999) Receptor-independent activators of heterotrimeric G-protein signaling pathways, *J. Biol. Chem. 274*, 33202−33205.
4. Clapham, D. E., and Neer, E. J. (1997) G protein $\beta\gamma$ subunits, *Annu. Rev. Pharmacol. Toxicol. 37*, 167−203.
5. Ford, C. E., Skiba, N. P., Bae, H., Daaka, Y., Reuveny, E., Shektar, L. R., Rosal, R., Weng, G., Yang, C.-S., Iyengar, R., Miller, R., Jan, L. Y., Lefkowitz, R. J., and Hamm, H. E. (1998) Molecular basis for interactions of G protein $\beta\gamma$ subunits with effectors, *Science 280*, 1271−1274.
6. Li, Y., Sternweis, P. M., Charnecki, S., Smith, T. F., Gilman, A. G., Neer, E. J., and Kozasa, T. (1998) Sites for G-α binding on the G protein β subunit overlap with sites for regulation of phospholipase C β and adenylyl cyclase, *J. Biol. Chem. 273*, 16265−16272.
7. Panchenko, M. P., Saxena, K., Li, Y., Charnecki, S., Sternweis, P. M., Smith, T. F., Gilman, A. G., Kozasa, T., and Neer, E. J. (1998) Sites important for PLC-β2 activation by the G protein $\beta\gamma$ subunit map to the sides of the β propeller structure, *J. Biol. Chem. 273*, 28298−28304.
8. Myung, C. S., and Garrison, J. C. (2000) Role of C-terminal domains of the G protein β subunit in the activation of effectors, *Proc. Natl. Acad. Sci. U.S.A. 97*, 9311−9316.
9. Yoshikawa, D. M., Bresciano, K., Hatwar, M., and Smrcka, A. V. (2001) Characterization of a phospholipase C β2-binding site near the amino terminal coiled-coil of G protein $\beta\gamma$ subunits, *J. Biol. Chem. 276*, 11246−11251.
10. Scott, J. K., Huang, S. F., Gangadhar, B. P., Samoriski, G. M., Clapp, P., Gross, R. A., Taussig, R., and Smrcka, A. V. (2001) Evidence that a protein−protein interaction "hot spot" on heterotrimeric G protein $\beta\gamma$ subunits is used for recognition of a subclass of effectors, *EMBO J. 20*, 767−776.
11. Delano, W. L. (2002) Unraveling hot spots in binding interfaces: progress and challenges, *Curr. Opin. Struct. Biol. 12*, 14−20.
12. Ma, B., Wolfson, H. J., and Nussinov, R. (2001) Protein functional libraries: hot spots, dynamics and combinatorial libraires, *Curr. Opin. Struct. Biol. 11*, 364−369.

13. Bonacci, T. M., Ghosh, M., Malik, S., and Smrcka, A. V. (2005) Regulatory interactions between the amino terminus of G-protein $\beta\gamma$ subunits and the catalytic domain of PLCβ2, *J. Biol. Chem. 280*, 10174−10181.
14. Goubaeva, F., Ghosh, M., Malik, S., Yang, J., Hinkle, P. M., Griendling, K. K., Neubig, R. R., and Smrcka, A. V. (2003) Stimulation of cellular signaling and G protein subunit dissociation by G protein $\beta\gamma$ subunit binding peptides, *J. Biol. Chem. 278*, 19634−19641.
15. Ghosh, M., Peterson, Y. K., Lanier, S. M., and Smrcka, A. V. (2003) Receptor and nucleotide exchange independent mechanisms for promoting G protein subunit dissociation, *J. Biol. Chem. 273*, 34747−34750.
16. Weng, G. Z., Li, J. R., Dingus, J., Hildebrandt, J. D., Weinstein, H., and Iyengar, R. (1996) G-β subunit interacts with a peptide encoding region 956−982 of adenylyl cyclase 2: Cross-linking of the peptide to free G $\beta\gamma$ but not the heterotrimer, *J. Biol. Chem. 271*, 26445−26448.
17. Chen, J., DeVivo, M., Dingus, J., Harry, A., Li, J., Sui, J., Carty, D. J., Blank, J. L., Exton, J. H., Stoffel, R. H., Inglese, J., Lefkowitz, R. J., Logothetis, D. E., Hildebrandt, J., and Iyengar, R. (1995) A region of adenylyl cyclase 2 critical for regulation by G protein $\beta\gamma$ subunits, *Science 268*, 1166−1169.
18. Koch, W. J., Inglese, J., Stone, W. C., and Lefkowitz, R. J. (1993) The binding site for the $\beta\gamma$ subunits of heterotrimeric G proteins on the β-adrenergic receptor kinase, *J. Biol. Chem. 268*, 8256−8260.
19. Kozasa, T., and Gilman, A. G. (1995) Purification of recombinant G proteins from Sf9 cells by hexahistidine tagging of associated subunits. Characterization of α_{12} and inhibition of adenylyl cyclase by α_z, *J. Biol. Chem. 270*, 1734−1741.
20. Otwinowski, Z., and Minor, W. (1997) Processing of X-ray diffraction data collected in oscillation mode, *Macromol. Crystallogr., Part A 276*, 307−326.
21. Storoni, L. C., Mccoy, A. J., and Read, R. J. (2004) Likelihood-enhanced fast rotation functions, *Acta Crystallogr., Sect. D: Biol. Crystallogr. 60*, 432−438.
22. Read, R. (2001) Pushing the boundaries of molecular replacement with maximum likelihood, *Acta Crystallogr., Sect. D: Biol. Crystallogr. 57*, 1373−1382.
23. Brunger, A. T., Adams, P. D., Clore, G. M., Delano, W. L., Gros, P., Grosse-Kunstleve, R. W., Jiang, J. S., Kuszewski, J., Nilges, M., Pannu, N. S., Read, R. J., Rice, L. M., Simonson, T., and Warren, G. L. (1998) Crystallography & NMR system: A new software suite for macromolecular structure determination, *Acta Crystallogr., Sect. D: Biol. Crystallogr. 54*, 905−921.
24. Adams, P. D., Pannu, N. S., Read, R. J., and Brunger, A. T. (1997) Cross-validated maximum likelihood enhances crystallographic simulated annealing refinement, *Proc. Natl. Acad. Sci U.S.A. 94*, 5018−5023.
25. Jones, T. A., Zou, J. Y., Cowan, S. W., and Kjeldgaard, M. (1991) Improved methods for building protein models in electron-density maps and the location of errors in these models, *Acta Crystallogr. A 47*, 110−119.
26. Laskowski, R. A., Macarthur, M. W., Moss, D. S., and Thornton, J. M. (1993) Procheck-A program to check the stereochemical quality of protein structures, *J. Appl. Crystallogr. 26*, 283−291.
27. Smrcka, A. V., and Scott, J. K. (2002) Discovery of ligands for $\beta\gamma$ subunits from phage-displayed peptide libraries, *Methods Enzymol. 344*, 557−576.
28. Sarvazyan, N. A., Remmers, A. E., and Neubig, R. R. (1998) Determinants of Giα and $\beta\gamma$ binding: Measuring high affinity interactions in a lipid environment using flow cytometry, *J. Biol. Chem. 273*, 7934−7940.
29. Sondek, J., Bohm, A., Lambright, D. G., Hamm, H. E., and Sigler, P. B. (1996) Crystal structure of a G-protein $\beta\gamma$ dimer at 2.1 Å resolution, *Nature 379*, 369−374.
30. Wall, M. A., Coleman, D. E., Lee, E., Iniguez-Lluhi, J. A., Posner, B. A., Gilman, A. G., and Sprang, S. R. (1995) The structure of the G protein heterotrimer G$i\alpha_1\beta_1\gamma_2$, *Cell 83*, 1047−1058.
31. Gaudet, R., Bohm, A., and Sigler, P. B. (1996) Crystal structure at 2.4 angstroms resolution of the complex of transducin $\beta\gamma$ and its regulator, phosducin, *Cell 87*, 577−588.
32. Loew, A., Ho, Y. K., Blundell, T., and Bax, B. (1998) Phosducin induces a structural change in transducin $\beta\gamma$, *Structure 6*, 1007−1019.
33. Lambright, D. G., Sondek, J., Bohm, A., Skiba, N. P., Hamm, H. E., and Sigler, P. B. (1996) The 2.0 Å crystal structure of a heterotrimeric G protein, *Nature 379*, 311−319.
34. Lodowski, D. T., Pitcher, J. A., Capel, W. D., Lefkowitz, R. J., and Tesmer, J. J. G. (2003) Keeping G proteins at bay: A complex between G protein-coupled receptor kinase 2 and G$\beta\gamma$, *Science 300*, 1256−1262.
35. Bogan, A. A., and Thorn, K. S. (1998) Anatomy of hot spots in protein interfaces, *J. Mol. Biol. 280*, 1−9.
36. Clackson, T., and Wells, J. A. (1995) A hot-spot of binding-energy in a hormone-receptor interface, *Science 267*, 383−386.
37. Delano, W. L., Ultsch, M. H., de Vos, A. M., and Wells, J. A. (2000) Convergent solutions to binding at a protein−protein interface, *Science 287*, 1279−1283.
38. Zhang, L., Li, Z., Yan, J., Pradhan, P., Corpora, T., Cheney, M. D., Bravo, J., Warren, A. J., Bushweller, J. H., and Speck, N. A. (2003) Mutagenesis of the runt domain defines two energetic hot spots for heterodimerization with the core binding factor β subunit, *J. Biol. Chem. 278*, 33097−33104.
39. Chen, Y., Weng, G., Li, J., Harry, A., Pieroni, J., Dingus, J., Hildebrant, J. D., Guarnieri, F., Weinstein, H., and Iyengar, R. (1997) A surface on G protein β subunit involed in interactions with adenylyl cyclases, *Proc. Natl. Acad. Sci U.S.A. 94*, 2711−2714.
40. Wall, M., Posner, B., and Sprang, S. (1998) Structural basis of activity and subunit recognition in g protein heterotrimers, *Structure 6*, 1169−1183.
41. Agler, H. L., Evans, J., Colecraft, H. M., and Yue, D. T. (2003) Custom distinctions in the interaction of G-protein β subunits with N-type (CaV2.2) versus P/Q-type (CaV2.1) calcium channels, *J. Gen. Physiol. 121*, 495−510.

BI050655I